JOURNAL OF Materials CHEMISTRY

Lead-free piezoelectric ceramics in the $(1 - x)Sr_2NaNb_5O_{15}$–$xCa_2NaNb_5O_{15}$ ($0.05 \leqslant x \leqslant 0.35$) system†

Rong-Jun Xie and Yoshio Akimune*

Smart Structure Research Center, National Institute of Advanced Industrial Science and Technology, Tsukuba Central 2, Umezono 1-1-1, Tsukuba, Ibaraki 305-8568, Japan. E-mail: y-akimune@aist.go.jp

Received 22nd March 2002, Accepted 28th June 2002
First published as an Advance Article on the web 12th August 2002

The study investigating the electrical properties of dense lead-free piezoelectric ceramics in the $(1 - x)Sr_2NaNb_5O_{15}$–$xCa_2NaNb_5O_{15}$ (SCNN) system with x ranging from 0.05 to 0.35 is reported here. X-Ray diffraction patterns all showed a single tetragonal tungsten bronze phase, peak broadening being seen on increasing the Ca content. The lattice constant calculation indicated distortion and shrinkage of the crystal structure with Ca substitution. Dielectric spectra of each composition displayed two dielectric anomalies and diffusive phase transitions. The Curie temperature, T_c, shifted upward whereas the relative permittivity at T_c declined monotonically as the Ca content increased. Ferroelectric and piezoelectric properties of SCNN greatly depended on the Ca content. The composition with $x = 0.15$ exhibited the greatest polarization with $P_r = 3.0$ μC cm^{-2} and piezoelectric constant of $d_{33} = 96$ pC N^{-1}, whereas the compositions with $x = 0.30$ and 0.35 almost lost their ferroelectricity and piezoelectricity. This study apparently indicates that lead-free SCNN piezoelectric ceramics have potential for electromechanical applications.

Introduction

Lead-based piezoelectric ceramics with perovskite structure, *e.g.*, PZT and PMN-PT, exhibit extremely high relative permittivity, large remanent polarization and high piezoelectric coefficients, and thus are widely used as electromechanical devices (actuators, sensors and transducers).[1,2] However, there are two serious problems arising from the fabrication of lead-containing materials, *i.e.*, difficult control of processing atmosphere and environmental pollution. Therefore, the development of lead-free piezoelectric ceramics has attracted much attention in recent years.[3–9] To date, the lead-free piezoelectric ceramics that have been extensively studied belong to the perovskite (*e.g.* $BaTiO_3$ and $(NaBi)TiO_3$) and bismuth-layered (*e.g.* $Bi_4Ti_3O_{12}$) structures. Besides these two families, piezoelectricity has also been identified in the ferroelectric tungsten bronze family. Neurgaonkar *et al.*[10,11] have systematically investigated tungsten bronze ferroelectric crystals and demonstrated encouraging piezoelectric properties in such compounds. According to Neurgaonkar *et al.*, calcium-modified strontium sodium niobates, ($Sr_{2-x}Ca_xNaNb_5O_{15}$, $0.05 \leqslant x \leqslant 0.35$), are thought to be potential lead-free piezoelectric materials, which exhibit a large piezoelectric constant of $d_{33} = 270$ pC N^{-1}.

The tungsten bronze structure, having a chemical formula $(A1)_2(A2)_4(C)(B)_{10}O_{30}$, is typified by oxygen octahedra sharing their corners in a complex way to yield three types of openings: A (A1 and A2), C and B.[12] In the crystal structure the A1, A2, C and B sites are the 15-, 12-, 9-, and 6-fold coordinated oxygen octahedra sites respectively, where the A sites are occupied by Sr, Ba, Ca, Pb, K, or Na, the C sites by Li, and the B sites by either Nb or Ta. Tungsten bronze solid solutions can be obtained with either tetragonal (4*mm*) symmetry in the ferroelectric phase or orthorhombic (*mm*2) symmetry, which can be both ferroelectric and ferroelastic.[10,12] The polar unit of tungsten bronze compounds is the NbO_6 octahedron, and the polar axis of tetragonal bronzes is parallel to the *c*-axis or [001].[10,12] Ferroelectricity in these compounds arises from the interaction between the Nb atoms and the oxygen framework in the polar unit.[13,14]

Recently, the authors successfully obtained fully dense $Sr_{1.9}Ca_{0.1}NaNb_5O_{15}$ ceramics using a novel spark plasma sintering technique and discussed the relationship between their electrical properties and the processing parameters.[15,16] Further, the authors partially substituted Sr by Ca in the range of 5–35 at% and briefly reported the influence of the substitution on the ferroelectric properties of SCNN in a previous paper.[17] In the study reported here, we extended the previous work on the $(1 - x)Sr_2NaNb_5O_{15}$–$xCa_2NaNb_5O_{15}$ system and measured the piezoelectric properties. The effects of the Ca substitution for Sr on the crystal structure, density and electrical properties were analyzed and discussed.

Experimental

Materials preparation

Calcium-modified strontium sodium niobates, $Sr_{2-x}Ca_xNaNb_5O_{15}$, with x ranging from 0.05 to 0.35, were prepared by solid-state reaction. Reagent grade $SrCO_3$, Na_2CO_3, $CaCO_3$ and Nb_2O_5 were used as starting materials. The powder mixtures of the desired compositions were ball-milled with ZrO_2 ceramic balls and water-free ethanol as grinding media for 24 h. After drying at 60 °C, the mixed powders were crushed and then calcined at 1150 °C for 6 h in air. A single phase was confirmed for the calcined powders by the X-ray diffraction (XRD) technique.

Ceramic samples were prepared by spark plasma sintering. In a cylindrical carbon die with an inner diameter of 15 mm, the calcined powder (~4.5 g) was sintered at 1200 °C with a heating rate of 300 °C min^{-1} for 5 min in a vacuum (~1 Pa) under a pressure of 35 MPa using Dr. Sinter (Model SPS-1030, Sumitomo Coal Mining Co., Ltd., Kanagawa, Japan). After sintering, the electric power was shut off to allow the sample to rapidly cool to room temperature (about 1 min for cooling from 1200 °C to 600 °C). The sintered ceramics were subsequently annealed at 1000 °C for 10 h in air to eliminate

†Electronic supplementary information (ESI) available: further experimental data. See http://www.rsc.org/suppdata/jm/b2/b202923p/

 DOI: 10.1039/b202923p

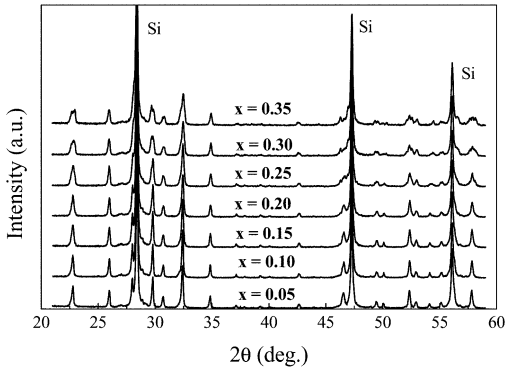

Fig. 1 X-Ray diffraction (XRD) patterns of $Sr_{2-x}Ca_xNaNb_5O_{15}$ ceramics with x varying in the range of 0.05–0.35, showing a single tetragonal tungsten bronze phase.

carbon contamination and oxygen deficiency during sintering. The weight loss of all samples was less than 1.5 wt%.

Microstructural characterization

Phase identification was analyzed using a Philips X'Pert X-ray diffractometer, operating at 50 mA and 40 kV using Cu-K_α radiation. The measured densities of sintered ceramics were determined using the Archimedes method, and theoretical densities of SCNN ceramics were calculated from the lattice parameter data. Microstructural observations were conducted using a scanning electron microscope (SEM, Model S-5000, Hitachi, Japan). Samples for SEM observation were prepared by cutting, machining and polishing with 0.25 μm diamond paste, and then thermally etching at 1200 °C for 20 min.

Property measurement

Electrodes were made on the large surfaces of the samples by coating them with a silver paste and then firing them at 750 °C for 30 min. Dielectric measurements were taken using an Agilent 4294A Impedance Analyzer over a temperature range of −100 to 350 °C and at various frequencies between 100 Hz and 1 MHz. The samples were heated and cooled at a rate of 2.5 °C min^{-1} and their dielectric data were recorded during the heating and cooling cycles. The electrical field-induced polarization was measured at room temperature using a standard Swayer-Tower circuit (Model FCE-1, Toyo Corporation, Japan) at 1 Hz; and the polarizations and the coercive fields were determined from the polarization–electrical field (P–E) hysteresis loops. Poling of the ceramic samples was performed by applying an electrical field of 10 kV cm^{-1} at 200 °C for 30 min and then cooling the samples to room temperature while maintaining the field. Piezoelectric properties were determined using the resonance–antiresonance frequency method.[18]

Results and discussion

Phase and structural analysis

Fig. 1 shows X-ray diffraction patterns of $Sr_{2-x}Ca_xNaNb_5O_{15}$ ($0.05 \leqslant x \leqslant 0.35$) ceramics. The patterns for most samples fit well with the Joint Committee on Powder Diffraction Standards Card No.34-0429, indicating a single tetragonal tungsten bronze phase without secondary phases being present. It has been reported that the crystal structure of SCNN is slightly distorted from the tetragonal structure and becomes orthorhombic at room temperature.[10] This is not consistent with our findings. It is possible that the cooling rate during sample preparation is so rapid that it suppresses the tetragonal-to-orthorhombic phase transition and, thus the tetragonal phase is maintained at room temperature,[15] as confirmed by the temperature dependence of the relative permittivity (shown later). Kimura *et al.* also did not observe the orthorhombic distortion in $(Ba_{1-x}Sr_x)_2NaNb_5O_{15}$ ceramics.[19] As seen in Fig. 1, the peaks become broader on increasing the Ca content and peak splitting occurs at $x = 0.35$. This indicates that (i) the incorporation of Ca^{2+} induces structural distortion and (ii) the solubility of Ca in the crystal lattice is up to 0.35. The lattice parameters of sintered SCNN ceramics are given in Table 1. As expected, the lattice constants, a and c, decrease monotonically on increasing the Ca content. Correspondingly, the lattice unit volume, V, is reduced as Ca^{2+} is introduced. The shrinkage of the unit cell can reasonably be attributed to the smaller ionic size of Ca^{2+} ($r_{Ca^{2+}} = 1.34$ Å, 12-CN) compared to that of Sr^{2+} ($r_{Sr^{2+}} = 1.44$ Å, 12-CN).[20] In the tungsten bronze system, the value of the axial ratio ($\sqrt{10}c/a$) is usually used to evaluate the distortion of the NbO_6 octahedra. Table 1 summaries the $\sqrt{10}c/a$ data and clearly shows that structural distortion is enhanced with increasing Ca content.

The measured and relative densities of sintered SCNN ceramics are given in Table 1. It is seen that all of the samples have densities higher than 97% of the theoretical density, suggesting that spark plasma sintering is an effective way to prepare highly dense SCNN ceramics at relatively low temperatures and within a short period. It is accepted that mass transportation or diffusion, which play key roles in densification, is greatly enhanced during spark plasma sintering.[15] Furthermore, the density is generally found to slightly decrease on increasing the Ca content. Fig. 2 shows typical SEM images of several specimens. These specimens feature a common microstructure that is dense, uniform and crack-free. The grain size of these specimens varies in the range of 2–6 μm despite the degree of substitution. This indicates that cation substitution has no appreciable influence on microstructure. So an effect of grain size on the electrical properties of SCNN ceramics can be ruled out in the following discussions.

Phase transition temperatures

The dielectric permittivity and the loss tangent as a function of temperature (−100–350 °C) at various frequencies (100 Hz–100 kHz) are given in Fig. 3. As can be seen, the dielectric

Table 1 Density and lattice parameters of $Sr_{2-x}Ca_xNaNb_5O_{15}$ ceramics

			Lattice constant/Å			
x	Density/g cm^{-3}	Relative density (%)	a	c	$\sqrt{10}c/a$	Volume/Å^3
0.05	4.96	98.4	12.3476 (12)	3.8947 (2)	0.9975	593.7974
0.10	5.00	99.4	12.3423 (9)	3.8940 (1)	0.9977	593.1811
0.15	4.99	99.4	12.3408 (8)	3.8933 (2)	0.9976	592.9273
0.20	4.97	99.2	12.3395 (13)	3.8916 (3)	0.9973	592.5408
0.25	4.96	99.2	12.3377 (10)	3.8896 (2)	0.9969	592.0668
0.30	4.92	98.8	12.3371 (9)	3.8876 (1)	0.9965	591.7071
0.35	4.83	97.2	12.3362 (11)	3.8865 (2)	0.9963	591.4541

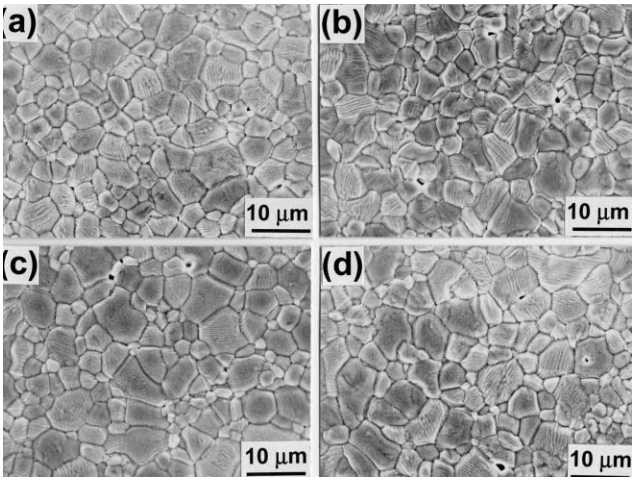

Fig. 2 SEM images of several $Sr_{2-x}Ca_xNaNb_5O_{15}$ ceramics: (a) $x = 0.05$, (b) $x = 0.15$, (c) $x = 0.25$ and (d) $x = 0.35$.

spectra of all specimens exhibit two broad dielectric anomalies over the temperature range of interest, which is in good agreement with the literature.[10,11] The high temperature anomaly is due to the paraelectric (4/*mmm*)–ferroelectric (4*mm*) transition (ferroelectric phase transition), and the low temperature one the ferroelectric (4*mm*)–ferroelastic (*mm*2) transition (ferroelastic phase transition).

The Curie temperature T_c, at which the ferroelectric phase transition occurs, is plotted as a function of the Ca concentration in Fig. 4. Thermal hysteresis of 6–16 °C is observed for each composition, indicating that the phase transition involves latent heat due to the coupling of strains associated with the phase transitions. T_c increases linearly as the Ca content increases, *i.e.*, from 279 °C for $x = 0.05$ to 297 °C for $x = 0.35$ upon cooling and from 287 °C for $x = 0.05$ to 316 °C for $x = 0.35$ upon heating. This linear relationship implies that the crystal structure of $Sr_2NaNb_5O_{15}$ (SNN) does not change as Ca is substituted for Sr. By extrapolating the Curie temperature to $x = 0$, we obtain T_c of 278 °C (cooling) and 282 °C (heating) for SNN, which are very close to the value of 270 °C reported by Van Uitert *et al.*[21] The increase in the Curie temperature can be attributed to the enhanced structural distortion that occurs with increasing Ca (see Table 1). The substitution of smaller Ca^{2+} for Sr^{2+} would result in a larger rattling space for the ions inside the oxygen octahedron, which increases the ionic displacements and thus the Curie temperature goes up. Unlike T_c, the second phase transition

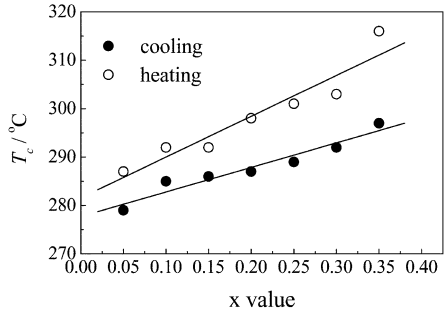

Fig. 4 The Curie temperature as a function of the Ca content.

temperature T_s (corresponding to the ferroelastic transition) displays a zig-zag curve on increasing the Ca content. T_s is −11, 0, −6, 7, 5, 6 and 2 °C for $x = 0.05$–0.35, respectively. Moreover, T_s for each composition is lower than room temperature, which confirms the presence of the tetragonal phase rather than the orthorhombic phase at room temperature.

Dielectric properties

Fig. 5 shows relative permittivities and the loss tangents at several temperatures as a function of the Ca content.

In Fig. 5(a), it is shown that the relative permittivities at T_c and T_s exhibit different tendencies with respect to the Ca content, and the relative permittivity of T_c is lower than that of T_s. At T_s and 25 °C, the relative permittivity nearly remains unchanged (except at $x = 0.05$). However, the relative permittivity at T_c decreases monotonically with increasing the Ca content, *i.e.*, from 1353 ($x = 0.05$) to 543 ($x = 0.35$). These results suggest that the Ca substitution strongly affects the ferroelectric transition. Generally, the relative permittivity is determined by four polarizations: atomic, ionic, dipolar, and space charge polarization. Under current experimental conditions, *i.e.*, high frequency and low electric field, only the atomic and ionic polarizations would contribute to the relative permittivity. Since the ionic size of Ca^{2+} is different from that of the substituted Sr^{2+} ions, increasing the Ca concentration would yield changes in both electronic and ionic polarizations. Ionic polarization strongly depends on the crystal structure (*e.g.*, density, lattice constant, and lattice volume). As shown in Table 1, incorporation of Ca^{2+} leads to reduced lattice constants, volume and density, causing a decrease in the ionic polarization. Further, partial substitution of Sr^{2+} by the smaller Ca^{2+} would result in a reduced electronic polarization. Therefore, the decline in relative permittivity at T_c with

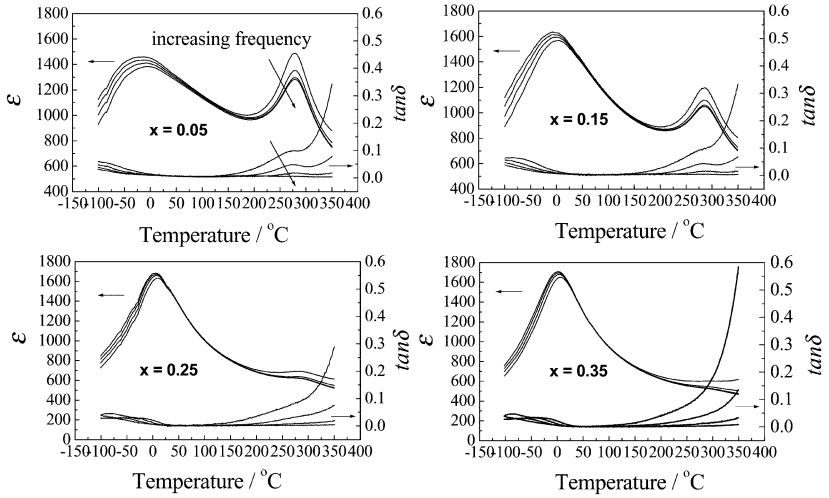

Fig. 3 Relative permittivity and the loss tangent of $Sr_{2-x}Ca_xNaNb_5O_{15}$ ceramics ($x = 0.05$, 0.15, 0.25 and 0.35) as a function of temperature at various frequencies (100, 1000, 10000 and 100000 Hz).

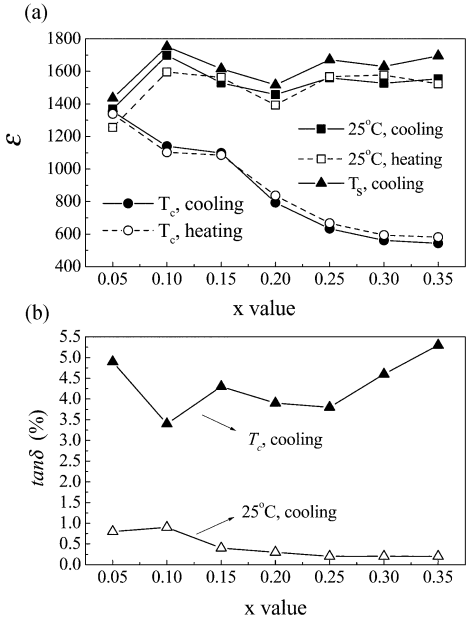

Fig. 5 The relative permittivity and loss tangent as a function of the Ca content.

increasing Ca can be attributed to the reduced ionic and electronic polarizations.

Similar to the relative permittivity, the loss tangent also shows two anomalies near the phase transition temperatures (see Fig. 3). The maximum dielectric loss temperatures are several degrees lower than their corresponding maximum relative permittivity temperatures. The losses at 25 °C and T_c are shown in Fig. 5(b) for each composition, measured at 1 kHz, upon cooling. The dielectric loss at T_c is in the range of 3.5–5.5% as the Ca content varies from 5 to 35 at%. At 25 °C, the dielectric loss is quite low, *e.g.* less than 0.9% for $x = 0.05$ and 0.10 and less than 0.4% for $x = 0.15$–0.35. The loss is nearly constant over a wide range of temperatures until the Curie temperature is achieved. At frequencies $\leqslant$100 Hz, the contribution of ionic conductivity to dielectric loss is appreciable at temperatures above 300 °C, resulting in a rapid increase in dielectric loss with increasing temperature.

Diffusive phase transition

Dispersion of the relative permittivity and loss tangent with frequency is clearly observed in the vicinity of both ferroelectric and ferroelastic phase transition temperatures for each composition. The maximum values of the relative permittivity and loss tangent shift to higher temperatures and decrease in magnitude as the measured frequency is increased, implying that the phase transitions of SCNN ceramics are diffusive. The differences between the relative permittivities at 100 Hz [ε_{100Hz}] and 1 MHz [ε_{1MHz}], $\Delta\varepsilon = \varepsilon_{100Hz} - \varepsilon_{1MHz}$, at both T_c and T_s are given in Table 2. It would seem that (i) the ferroelectric transition is more diffusive than the ferroelastic one, and (ii) the diffusive phase transition is less pronounced for compositions with higher Ca concentrations.

For a classic ferroelectric the relative permittivity above the Curie temperature follows the Curie–Weiss law:

$$\varepsilon = \frac{C}{T - \Theta} \tag{1}$$

where ε is the relative permittivity at T, C the Curie–Weiss constant, and Θ the Curie–Weiss temperature. The plots of $1/\varepsilon$ *vs.* T for several specimens are given in Fig. 6. It is found that for compositions of $x \geqslant 0.25$, the relative permittivity exhibits Curie–Weiss behavior in the temperature range immediately above T_c, whereas for compositions of $x < 0.25$,

Table 2 Dielectric characterization of $Sr_{2-x}Ca_xNaNb_5O_{15}$ ceramics

					$\varepsilon_{1MHz} - \varepsilon_{100Hz}$		
x	Θ/°C	T_{cw}/°C	$T_{cw} - T_c$/°C	$C/10^5$ °C	T_c	T_s	$\varepsilon_{25°C} \times P_s$
0.05	205	296	17	1.13	191	86	3789
0.10	198	301	16	1.11	145	155	4078
0.15	189	302	16	1.15	162	111	4587
0.20	129	301	14	1.31	107	85	3205
0.25	−75	297	8	2.33	82	89	2808
0.30	−222	294	2	3.45	82	86	31
0.35	−183	299	2	3.63	91	114	16

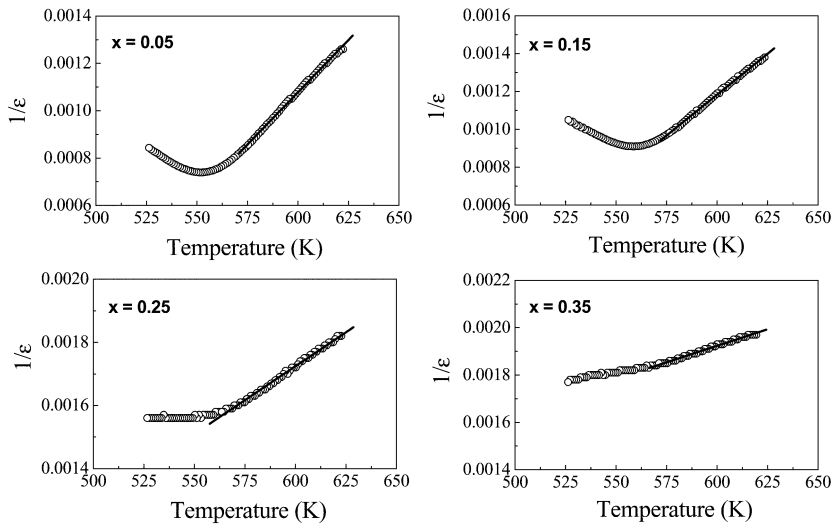

Fig. 6 Thermal variation of the inverse of the relative permittivity $1/\varepsilon$, at 1 kHz for $Sr_{2-x}Ca_xNaNb_5O_{15}$ ceramics ($x = 0.05$, 0.15, 0.25 and 0.35).

the relative permittivity deviates from the Curie–Weiss law over a wide range of temperatures above T_c. The Curie–Weiss temperature Θ, the Curie–Weiss constant C and the temperature at which the curve starts to follow the Curie–Weiss law T_{cw} for all specimens are presented in Table 2. The departure from the Curie–Weiss law suggests that the compositions with $x < 0.25$ have a characteristic of diffusion phase transition (DPT). In a previous paper,[17] the authors calculated the diffuseness of the phase transition for each composition using an empirical expression proposed by Uchino and Nomura[22] The diffusivity γ was found to be largest for the composition with $x = 0.15$ ($\gamma \sim 1.52$) and lowest for the compositions with $x = 0.30$ and 0.35 ($\gamma \sim 1.10$). γ values in the range of 1.10–1.52 indicate that the sintered ceramics are not relaxors, in contrast to other tungsten bronze oxides where a typical relaxor behavior was observed.[23,24] The mechanisms for the diffuse characteristics of tungsten bronze ferroelectrics, such as compositional inhomogeneities, cation ordering, or other structural defects, are well documented in the literature,[12,22–24] and these can also be applicable to the present system. The fact that Θ is far below T_c indicates that the ferroelectric transition is first order, which is also evidenced by observations of the thermal hysteresis of the dielectric properties.

Ferroelectric and piezoelectric properties

Electrically induced polarizations (P–E curves) of all the compositions were measured at room temperature. For compositions with $x \leqslant 0.25$, the P–E curves (not shown here) exhibit typical polarization–electric field hysteresis loops, which is a characteristic of ferroelectrics. The degree of hysteresis remains nearly constant with the Ca content up to 0.25. On further increment of the Ca content, both the degree of ferroelectric hysteresis and the polarizations reduce suddenly and markedly, which agrees well with the dielectric behavior. The spontaneous polarization (P_s), remanent polarization (P_r) and the coercive field (E_c) were determined from the hysteresis loops and are plotted as a function of the Ca content in Fig. 7. Note that the ferroelectric properties of SCNN ceramics initially increase with increasing Ca, reach maximum values at $x = 0.15$, and then decline gradually when $x > 0.15$. A significant decrease in ferroelectric properties is found for compositions with $x > 0.25$. The composition with $x = 0.15$ has the largest values of $P_s = 9.1$ μC cm^{-2}, $P_r = 3.0$ μC cm^{-2} and $E_c = 12.9$ kV cm^{-1}, respectively, whereas the compositions with $x = 0.30$ and 0.35 have values two-orders of magnitude smaller than those at $x = 0.15$.

The electromechanical coupling coefficients k_p and k_t, and the piezoelectric constant d_{33} as a function of the Ca content ($x \leqslant 0.25$) are shown in Fig. 8. Poled specimens with compositions of $x = 0.30$ and 0.35 give no piezoelectric response, so the piezoelectric properties of these two compositions are not available. Similar to the ferroelectric properties, the piezoelectric properties of SCNN ceramics increase on

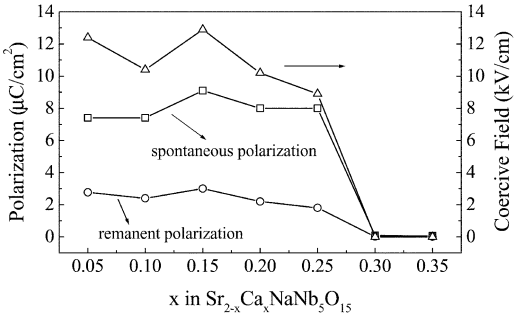

Fig. 7 Spontaneous polarization P_s, remanent polarization P_r and coercive field E_c as a function of Ca content.

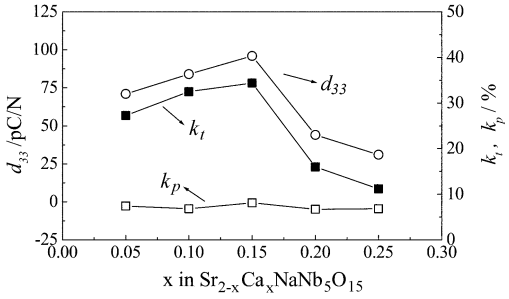

Fig. 8 Electromechanical coupling coefficients k_p and k_t, and the piezoelectric constant d_{33}, as a function of Ca content.

increasing the Ca content until the values reach a maximum at $x = 0.15$, and then reduce sharply (except k_t) with further increases in the Ca content. The values of k_p, k_t and d_{33} for the composition of $x = 0.15$ are 34.4%, 8.1% and 96 pC N^{-1}, respectively, and those values are 11.2%, 6.8% and 31 pC N^{-1} for the composition of $x = 0.25$.

The above observations show that the Ca substitution exerts a large influence on ferroelectric and piezoelectric properties of SCNN ceramics, and the largest values of the polarization and piezoelectric constant occur at 15 at% Ca substitution. This may be due to the changes in the crystal structure and polarizability that occur as Ca is incorporated. As shown in Table 1, the distortion of crystal lattice is enhanced and the rattling space is enlarged by increasing the Ca content, which causes a higher Curie temperature and greater spontaneous polarization. This is true when the Ca concentration is $\leq$15at%, as observed in Figs. 4 and 7. Further introduction of Ca into the structure, however, leads to decreased polarizations, probably due to (i) smaller polarizability of Ca in comparison with that of Sr and (ii) reduced stability of the tungsten bronze structure (see the peak broadening and splitting in Fig. 1). For piezoelectric properties, the piezoelectric coefficient d_{33} can generally be expressed as a function of its relative permittivity ε and polarization P

$$d_{33} = 2Q_{eff}\varepsilon_0\varepsilon P \quad (2)$$

where Q_{eff} is the effective electrostriction coefficient which is related to the domain structure. For the ceramics studied here, Q_{eff} is considered to be nearly constant since the domain structure of SCNN cannot be altered significantly by Ca substitution. Therefore, the piezoelectric coefficient is greatly dependent on the relative permittivity and polarization in the present system. The values of εP for each composition are given in Table 2 and show a trend similar to that for the measured piezoelectric coefficient.

Conclusions

Dense piezoelectric ceramics in the $(1 - x)Sr_2NaNb_5O_{15}$–$xCa_2NaNb_5O_{15}$ system were prepared by spark plasma sintering, and their structure and electrical properties were investigated as a function of the Ca content. The Ca substitution for Sr in SCNN had a large influence on the electrical properties due to changes in the crystal lattice and polarizability. The composition with $x = 0.15$ exhibited the largest ferroelectric and piezoelectric properties with values of $P_s = 9.1$ μC cm^{-2}, $P_r = 3.0$ μC cm^{-2} and $d_{33} = 96$ pC N^{-1}.

The present work shows that SCNN ceramics, which are environmentally friendly, are potential piezoelectric materials suitable for electromechanical applications in actuators and sensors. Research is now underway to further improve their piezoelectric properties, making their practical use possible.

Acknowledgements

The authors would like to acknowledge the Japanese Science and Technology Cooperation for financial support. Experimental support from Mr K. Matsuo and T. Sugiyama are greatly appreciated.

References

1 B. Jaffe, W. R. Cook, Jr., and H. Jaffe, *Piezoelectric Ceramics*, Academic Press, New York, 1971.
2 G. H. Haertling, *J. Am. Ceram. Soc.*, 1999, **82**, 797.
3 J. Ravez, C. Broustera and A. Simon, *J. Mater. Chem.*, 1999, **9**, 1609.
4 T. Takenaka and K. Sakata, *Ferroelectrics*, 1989, **95**, 153.
5 T. Takenaka, K. Sakata and K. Toda, *Ferroelectrics*, 1990, **106**, 375.
6 T. Takenaka, K. I. Maruyama and K. Sakata, *Jpn. J. Appl. Phys. B*, 1991, **30**(9), 2236.
7 Y. M. Chiang, G. W. Farrey and A. N. Soukhojak, *Appl. Phys. Lett.*, 1998, **73**, 3683.
8 E. C. Subbarao, *Phys. Rev.*, 1961, **122**, 804.
9 L. Sagalowicz, F. Chu, P. D. Martin and D. Damjanovic, *J. Appl. Phys.*, 2000, **88**, 7258.
10 R. R. Neurgaonkar, J. R. Oliver, W. K. Copy, L. E. Cross and D. Viehland, *Ferroelectrics*, 1994, **160**, 265.
11 R. R. Neurgaonkar, W. F. Hall, J. R. Oliver, W. W. Ho and W. K. Copy, *Ferroelectrics*, 1988, **87**, 167.
12 M. E. Lines and A. M. Glass, *Principles and Applications of ferroelectrics and Related Materials*, Clarendon Press, Oxford, 1977.
13 M. H. Francombe, *Acta Crystallogr.*, 1960, **13**, 131.
14 P. B. Jamieson, S. C. Abrahams and J. L. Bernstein, *J. Chem. Phys.*, 1969, **50**, 4352.
15 R. J. Xie, Y. Akimune, R. P. Wang, K. Matsuo, T. Sugiyama and N. Hirosaki, submitted for publication in *J. Am. Ceram. Soc*.
16 R. J. Xie, Y. Akimune, R. P. Wang and N. Hirosaki, submitted for publication in *J. Am. Ceram. Soc*.
17 R. J. Xie, Y. Akimune, K. Matsuo, T. Sugiyama, N. Hirosaki and T. Sekiya, *Appl. Phys. Lett.*, 2002, **80**, 835.
18 H. Meitzer, D. Berlincourt, G. A. Goquin, F. S. Welsh III, H. F. Tiersten and A. W. Warner, *IEEE Standard on Piezoelectricity*, American National Standards Institute, Washington D.C., 1976.
19 M. Kimura, T. Minamikawa, A. Ando and Y. Sakabe, *Jpn. J. Appl. Phys.*, 1997, **36**, 6051.
20 R. D. Shannon, *Acta Crystallogr., Sect. A*, 1976, **32**, 751.
21 L. G. Van Uitert, J. J. Rubin, W. H. Grodkiewicz and W. A. Bonner, *Mater. Res. Bull.*, 1969, **4**, 63.
22 K. Uchino and S. Nomura, *Ferroelectric Lett.*, 1982, **44**, 55.
23 A. M. Glass, *J. Appl. Phys.*, 1969, **40**, 4699.
24 L. E. Cross, *Ferroelectrics*, 1994, **151**, 305.
25 L. E. Cross, *Ferroelectrics*, 1987, **76**, 241.